Rotationally Induced Hydrodynamics: Fundamentals and Applications to High-Speed Bioassays

Gufeng Wang,[1] Jeremy D. Driskell,[2] April A. Hill,[3] Eric J. Dufek,[4] Robert J. Lipert,[1] and Marc D. Porter[4]

[1]Institute for Physical Research and Technology and Ames Laboratory–U.S. Department of Energy, Iowa State University, Ames, Iowa 50011; email: blipert@ameslab.gov

[2]Department of Infectious Diseases, University of Georgia, Athens, Georgia 30602

[3]Materials Science and Engineering Center, The Pennsylvania State University, University Park, Pennsylvania 16802

[4]Nano Institute of Utah and the Departments of Chemistry, Chemical Engineering, Bioengineering, and Pathology, University of Utah, Salt Lake City, Utah 84108; email: marc.porter@utah.edu

Annu. Rev. Anal. Chem. 2010. 3:387–407

First published online as a Review in Advance on April 2, 2010

The *Annual Review of Analytical Chemistry* is online at anchem.annualreviews.org

This article's doi: 10.1146/annurev.anchem.111808.073644

1936-1327/10/0719-0387$20.00

Key Words

rotating disk electrode, mass transport, immunoassay, gold nanoparticles (GNPs), surface-enhanced Raman scattering (SERS), atomic force microscopy (AFM), extrinsic Raman labels (ERLs)

Abstract

Bioassays are indispensable tools in areas ranging from fundamental life science research to clinical practice. Improving assay speed and levels of detection will have a profound impact in all of these areas. We recently developed a rapid, sensitive format for immunosorbent assays that expedites antigen mass transport by rotating the capture substrate. This review outlines the theoretical foundation of rotationally induced hydrodynamics and its application in heterogeneous assays. We describe a general solution that solves the rates of immunoreactions on rotating capture substrates, taking into account both diffusion and the rate of reaction between antibody and antigen. The general solution applies to a wide range of rotation rates, including mass transport–limited to reaction rate–limited assays, and is validated experimentally. We discuss several applications that demonstrate how immunoassays can be tailored to increase speed as well as lower the limit of detection of viral particles, pathogens, toxins, and proteins.

1. INTRODUCTION

LOD: limit of detection

SERS: surface-enhanced Raman scattering

AFM: atomic force microscopy

Bioassays are essential tools in basic life science research, drug discovery, human and veterinary diagnostics, food and environmental safety, and bioterrorism prevention (1–7). Although such assays are already a mainstay in the diagnostics arena, enhancements in sample throughput, analysis time, and levels of detection will clearly advance early disease diagnosis, improve patient prognosis, reduce outbreaks, and decrease hospitalization. We have recently shown that the hydrodynamics induced by substrate rotation provide an effective means to (*a*) increase the speed of heterogeneous immunoassays while (*b*) simultaneously lowering the limit of detection (LOD). This review focuses on the theory and application of this new immunoassay format.

Many of today's assays rely on fluorescence for detection, and optical absorbance is still commonplace for enzyme-linked immunosorbent assays. Motivated by the need to decrease the LOD, investigators have developed several innovative approaches to readout, including techniques based on nanowires (8–10), surface plasmon resonance (11–16), quantum dots (17–22), microcantilevers (23–25), surface-enhanced Raman scattering (SERS) (5, 26–39), and atomic force microscopy (AFM) (40–44). These techniques are capable of detecting tens to hundreds of antigens after capture on a solid phase, which can translate to LODs in the femtomolar range. However, the delivery of antigen to the sensing surface often relies on diffusion as the mode of mass transport (**Figure 1**), which results in long incubation times (i.e., several hours) because biological analytes have small diffusion coefficients due to their large sizes (45). Consequently, the accumulation of a detectable level of analyte at the sensing surface at concentrations below the femtomolar range is not possible on a realistic time scale.

Several approaches for increasing reactant flux have been investigated as ways to overcome this obstacle. These strategies leverage the fact that antibody-antigen binding kinetics are typically fast relative to mass transport (46–52). Magnetic field–assisted flux (53), confinement of the fluid-flow profile to a thin layer above the sensing surface (54, 55), and elevations in temperature to decrease solution viscosity (56) have all been explored. Despite decreasing assay time, questions concerning how such modalities can best be used and what LODs are achievable remain only partially answered. Furthermore, the practical utility of magnetic field–based approaches is potentially confounded by the expense of magnetic labels and reagents. Two of the most mature methods of increasing flux include electric field–driven assays (57–60) and lateral-flow assays (61–68).

Electric fields can be used to drive the transport of charged species and have been employed to reduce DNA-hybridization assays (60) and heterogeneous immunoassays to only a few minutes (57). Targets can also be manipulated electrophoretically to specific locations in a microelectrode array (57, 58) or electroosmotically in microchannels (59). These approaches, however, are not

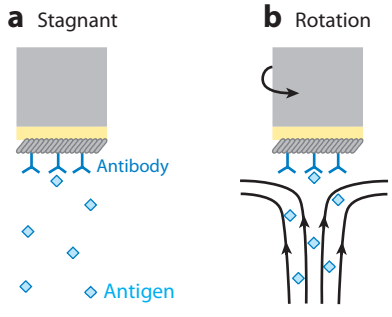

Figure 1

Schematic representation of antigen binding under (*a*) stagnant and (*b*) rotation conditions.

broadly applicable because different targets have different isoelectric points and therefore have mobilities that vary with pH. Issues related to the ionic strength of the solution must also be taken into account.

Lateral-flow, or immunochromatographic, assays have already been incorporated into many commercial systems (61–68). Lateral-flow assays employ a porous membrane (e.g., nitrocellulose) as a solid phase with a localized region of immobilized antibody. Capillary forces drive the liquid through the membrane, and the antigen and tracer are extracted and concentrated in the capture zone. This method has been used to monitor drugs, toxins, hormones, proteins, and pathogens (63). The popularity of this so-called dipstick configuration lies in its ease of use, speed, and portability. Nonetheless, these assays are semiquantitative at best, and signal saturation is common. LODs and the ability to multiplex can also be problematic.

This review discusses an approach that employs rotation-induced flux (**Figure 1**) as a means to overcome many of these barriers. Rotation-induced flux is a well-established method for quantitatively manipulating mass transport and is a mainstay in electrochemical research (69–71). We recently published a series of papers describing the development, theory, application, and advantages of using a rotating capture substrate as a new immunoassay format (72–74). Herein we describe a model of antibody-antigen binding kinetics at a rapidly rotating capture substrate, along with studies that validate the model. Note that although the experiments conducted in our laboratory relied largely on AFM and SERS for detection, the overall approach can be implemented with almost any type of assay and readout modality. The following sections also include examples in which a rotating capture substrate is used to detect viruses, pathogens, toxins, and proteins, highlighting the ability to decrease assay time, reduce nonspecific binding, and enable standard-free quantification of important antigens.

Rotation-induced flux: convective flow induced by rotation of substrate

Nonspecific binding: the undesirable case in which a nontarget antigen or secondary antibody binds to the capture antibody

2. THEORY

We developed our model by considering two components of the assay mechanism: (*a*) antigen binding to an antibody-modified substrate and (*b*) the rate of reactant delivery (i.e., the flux of reactant to the substrate). The former component embodies the rates of antigen-antibody association and dissociation. The latter component formulates the reactant flux in terms of diffusion- or convection-controlled mass transport. The convective model is based on the hydrodynamics introduced by substrate rotation and takes advantage of the quantitative formulations that have been a hallmark of the use of rotating disk electrodes in electrochemistry (69–71).

2.1. Antibody-Antigen Binding

Consider an antibody-antigen binding reaction at a capture surface,

$$S_{Ab} + Ag \Leftrightarrow S_{Ab-Ag}, \tag{1}$$

where S_{Ab} is the immobilized antibody on the capture surface, Ag is the antigen, and S_{Ab-Ag} is the surface-bound antibody-antigen complex. The equilibrium binding constant K is

$$K = \frac{k_{on}}{k_{off}} = \frac{\Gamma}{(S^0_{Ab} - p\Gamma)[Ag]}, \tag{2}$$

where k_{on} (liter mol^{-1} s^{-1}) and k_{off} (liter s^{-1}) are the association- and dissociation-rate constants, Γ is the captured antigen concentration on the surface (mol m^{-2}), $[Ag]$ is the antigen concentration at equilibrium (mol liter^{-1}), S^0_{Ab} is the initial surface antibody concentration (mol m^{-2}), and p is

the ratio of S^0_{Ab} to the jamming limit of the antigen S^0_{Ag}:

$$p = S^0_{Ab}/S^0_{Ag}. \tag{3}$$

This factor is introduced when the antigen is larger than the antibody. It is needed when packing of antigen is limited by the size of the antigen and not by the size of the antibody.

2.2. Static Conditions

The flux of reactant to a planar substrate can be quantitatively formulated for systems that meet the following boundary conditions. Condition 1 dictates that the reactant be homogeneously distributed throughout the solution before the experiment begins. Condition 2, the semi-infinite condition, requires that the solution at some position removed from the substrate remain unaffected over the course of the experiment.

In quiet solution, the linear-diffusion equation is

$$\frac{\partial C}{\partial t} = D\frac{\partial^2 C}{\partial x^2}, \tag{4}$$

where D is the diffusion coefficient of the antigen ($m^2\ s^{-1}$), C is the analyte concentration, t is time (s), and x is the distance in solution from the surface (i.e., $x = 0$ defines the substrate surface). In electrochemistry (69, 71), the observed current in quiet solution is directly linked to the diffusional flux (J_{diff}, mol $m^{-2}\ s^{-1}$) of a redox species at the electrode surface,

$$J_{diff} = \frac{D^{1/2}C^b}{\pi^{1/2}t^{1/2}}, \tag{5}$$

where C^b is the bulk concentration of analyte. If we assume that the concentration of reactant is continually driven to zero at the electrode surface, the result is the well-known Cottrell equation,

$$i_d = \frac{nFAD^{1/2}C^b}{\pi^{1/2}t^{1/2}}, \tag{6}$$

where i_d is the diffusion-limited current, n is the redox stoichiometry, F is Faraday's constant, and A is the area of the electrode. Integration of Equation 6 then yields the accumulated charge, Q_d, as a function of electrolysis time:

$$Q_d = \frac{2nFAD^{1/2}C^b t^{1/2}}{\pi^{1/2}}. \tag{7}$$

The same approach can be applied to a heterogeneous immunoassay by adding one more boundary condition, namely that the binding sites on the capture substrate not be saturated with antigen. Below, we show that the resulting theory allows the quantity of extracted antigen to be predicted, and we also underscore the importance of the diffusion coefficient and the need for increased mass transport for large molecules.

Using these three boundary conditions, one can calculate the uptake of antigen over time through a simple modification of Equation 7:

$$\Gamma = \frac{2D^{1/2}C^b t^{1/2}}{\pi^{1/2}}. \tag{8}$$

This equation shows that accumulation of antigen is directly proportional to $D^{1/2}$, indicating that a 100-fold difference in D translates to a 10-fold difference in Γ. Equation 8 also shows that Γ increases linearly with $t^{1/2}$.

2.3. Rotation-Induced Convection

At a rotating disk, mass transport combines diffusive and convective flow. The convective-diffusion equation for linear flow toward the surface (i.e., the negative x direction) is

$$\frac{\partial C}{\partial t} = D\frac{\partial^2 C}{\partial x^2} - v_x\frac{\partial C}{\partial x}, \tag{9}$$

where v_x is the flow velocity in the x direction. At steady state, the velocity profile is

$$v_x = -0.51\omega^{2/3}V^{-1/2}x^2. \tag{10}$$

Here, V is the kinematic viscosity of the liquid, and ω is angular velocity (rad s^{-1}) (75).

In electrochemistry, when the current at a rotating disk electrode is limited by mass transport, the concentration near the electrode surface is independent of time:

$$\frac{\partial C}{\partial t} = 0. \tag{11}$$

We can then integrate and solve Equation 9 to yield

$$C^b = -\left(\frac{\partial C}{\partial x}\right)_{x=0} 1.61D^{1/3}\omega^{-1/2}V^{1/6} \tag{12}$$

because the flux of reactant under the conditions of convection (J_{conv}, mol m^{-2} s^{-1}) at the surface is

$$J_{conv} = -D\left(\frac{\partial C}{\partial x}\right)_{x=0}. \tag{13}$$

Thus, substitution of Equation 13 into Equation 12 gives

$$J_{conv} = C^b\frac{D}{1.61D^{1/3}\omega^{-1/2}V^{1/6}} = C^b\frac{D}{\delta}, \tag{14}$$

where δ is the diffusion-layer thickness (m)

$$\delta = 1.61V^{1/6}D^{1/3}\omega^{-1/2}. \tag{15}$$

The same solutions (Equations 12–15) also apply to binding reactions at the surface of a rotating capture substrate if the binding reaction is mass-transport limited and the accumulation of antigen can be neglected (e.g., at early incubation times). J_{conv} can also be written as

$$J_{conv} = \frac{\Delta\Gamma}{\Delta t}. \tag{16}$$

When the rate of mass transport to the surface surpasses the rate of binding, the interfacial reaction kinetics must be considered when solving Equation 9; that is, the association and dissociation of the surface complex should be included in a complete solution for the heterogeneous immunoreaction. Specifically, the boundary condition at the capture surface is

$$-D\left(\frac{\partial C}{\partial x}\right)_{x=0} = k_{on}(S^0_{Ab} - p\Gamma)C_1 - k_{off}\Gamma, \tag{17}$$

where C_1 is the antigen concentration in the liquid immediately adjacent to the surface. To solve Equation 9, the quasi-static condition approximation must be applied (Equation 11). Again, we can integrate and solve Equation 9 for the net flux at the surface:

$$C^b - C_1 = -\left(\frac{\partial C}{\partial x}\right)_{x=0} 1.61D^{1/3}\omega^{-1/2}V^{1/6}. \tag{18}$$

Mass-transport limited: refers to the accumulation of antigen on the surface being governed by the rate at which the antigen reaches the surface; antibody-antigen binding is relatively fast in comparison

Because

$$J_{conv} = \frac{\partial \Gamma}{\partial t} = D\frac{C^b - C_1}{\delta}, \tag{19}$$

combining Equations 17 and 18 yields

$$C_1 = \frac{C^b D/\delta + k_{off}\Gamma}{k_{on}(S^0_{Ab} - p\Gamma) + D/\delta}. \tag{20}$$

Note that C_1 is time dependent because Γ increases with time. As shown below, it is reasonable to assume that C_1 is a constant at short time scales.

Equation 20 can be simplified by recognizing that Γ is insignificant at short time scales, which gives

$$C_1 = \frac{C^b}{1 + k_{on}S^0_{Ab}/(D/\delta)}. \tag{21}$$

Next, we can substitute Equation 21 into Equation 19, leaving

$$J_{conv} = \frac{\partial \Gamma}{\partial t} = \frac{k_{on}S^0_{Ab}}{1 + k_{on}S^0_{Ab}/(D/\delta)}C^b. \tag{22}$$

Integration of Equation 22 shows that Γ is linearly proportional to t at short incubation times:

$$\Gamma = \frac{k_{on}S^0_{Ab}}{1 + k_{on}S^0_{Ab}/(D/\delta)}C^b t. \tag{23}$$

To determine k_{on} and D, Equation 23 can be rearranged to form

$$\frac{C^b t}{\Gamma} = \frac{\delta}{D} + \frac{1}{k_{on}S^0_{Ab}}. \tag{24}$$

Finally, substitution of Equation 15 into Equation 24 gives

$$\frac{C^b t}{\Gamma} = \frac{1.61V^{1/6}}{D^{2/3}}\frac{1}{\omega^{1/2}} + \frac{1}{k_{on}S^0_{Ab}}. \tag{25}$$

Equation 25 shows that $1/\Gamma$ is proportional to $1/\omega^{1/2}$. We can therefore determine D and $k_{on}S^0_{Ab}$ by measuring Γ at several angular velocities and by using a linear-regression analysis to establish the slope and intercept of the plot. If we know or can reasonably estimate S^0_{Ab}, then k_{on} can be determined. Note that under extremely low rotation conditions, the hydrodynamic boundary approaches the size of the substrate, and the approximations made in the solutions of Equation 9 are no longer valid (69).

3. EXPERIMENTAL VALIDATION OF THEORY: MODEL SYSTEM FOR ANTIBODY-ANTIGEN BINDING KINETICS AT A ROTATING CAPTURE SUBSTRATE

3.1. Mass Transport– Versus Reaction Rate–Limited Binding

In Section 2, we developed general solutions for the binding kinetics at a capture substrate rotated from low to extremely high speeds. Equation 22 shows that two terms, $k_{on}S^0_{Ab}$ and D/δ, dominate the rate of reactant accumulation. The former term is a measure of the binding rate, and the latter is a measure of the mass-transport rate. The ratio of the two terms, the dimensionless Damköhler number ($D_a = k_{on}S^0_{Ab}\delta/D$), is a good measure of whether the reaction is mass-transport limited or reaction-rate limited. When $D_a \gg 1$ surface accumulation is mass-transport limited, whereas when $D_a \ll 1$ accumulation is limited by the rate of reaction between antigen and antibody.

The impact of the three kinetic regimes can be more precisely formulated. When $k_{on}S^0_{Ab}$ is much larger than D/δ ($D_a \gg 1$), accumulation is limited by mass transport. Equation 22 then reduces to the product of

$$J_{conv} = \frac{\Delta\Gamma}{\Delta t} = \frac{D}{\delta}C^b. \quad (26)$$

Using Equation 15, we can recast Equation 26 as

$$J_{conv} = \frac{\Delta\Gamma}{\Delta t} = \frac{D^{2/3}C^b}{1.61V^{1/6}}\omega^{1/2}. \quad (27)$$

In this case, the flux of the antigen at the capture surface is proportional to $\omega^{1/2}$.

When $k_{on}S^0_{Ab}$ is much smaller than D/δ ($D_a \ll 1$), accumulation is limited by the reaction rate, and Equation 22 reduces to

$$J_{conv} = \frac{\Delta\Gamma}{\Delta t} = k_{on}S^0_{Ab}C^b. \quad (28)$$

Interestingly, the flux of the antigen onto the capture surface is independent of ω.

When $k_{on}S^0_{Ab}$ is similar to D/δ, binding falls in the regime of intermediate reaction kinetics. Both terms contribute to the rate of antigen accumulation, and Equation 22 must be used. One therefore expects that a plot of Γ versus $\omega^{1/2}$ would (*a*) be linear at low ω, that is, when mass transport is limiting and the D/δ term dominates; (*b*) start to level off at higher ω, that is, when both the reaction rate and mass transport affect the binding rate; and (*c*) eventually become independent of ω, specifically when the binding reaction rate is limiting and the $k_{on}S^0_{Ab}$ term becomes controlling.

3.2. Capturing Gold Nanoparticles: An Atomic Force Microscopy Study

To test these predictions, 30-nm gold nanoparticles (GNPs) were modified with an antibody [anti–mouse immunoglobin G (IgG)] to act as a model analyte and were exposed to an antigen (mouse IgG)-coated capture substrate. AFM was then used to directly enumerate the captured GNPs to determine Γ. These results are presented in the 5 × 5 μm images in **Figure 2*a–b*** for capture substrates rotated at different speeds for 10 min in a 3.6×10^9 particles ml^{-1} suspension. As is evident, the number of captured GNPs increases with ω, consistent with the rotational control of δ and, in turn, binding rates.

The other three images in **Figure 2** provide further support for the development and expectations of Equations 22 and 23. **Figure 2*i*** shows a surface that is saturated with nanoparticles following static incubation in a high concentration of GNPs for 16 h. The high packing density of GNPs demonstrates that the surface is far from saturated after the 10-min rotations. Furthermore, the images in **Figure 2*j*,*k*** show an increase in Γ for 20- and 30-min rotations at 800 rpm. The numbers of captured GNPs per 25 μm^2 are 253 ± 8 and 320 ± 15, respectively, compared to 128 ± 14 GNPs for a 10-min rotation at 800 rpm. This trend indicates that Γ is linearly dependent on t. These data validate the low–surface concentration criterion employed in the development and use of Equations 22 and 23.

At a more detailed level, the experimentally determined flux ($J = \Delta\Gamma/\Delta t$) of GNPs is plotted in **Figure 3** as a function of $\omega^{1/2}$. J roughly follows a linear dependency on $\omega^{1/2}$ at the lower rotation speeds, which indicates mass transport–limited kinetics per Equation 27. When the rotation speed surpasses ~25 rad s^{-1} (~240 rpm), the plot deviates from linearity, which shows that the mass transport–limited condition is no longer valid. Moreover, a best fit of Equation 22 to the experimental data suggests that J will reach a limiting value at a large rotation rate, as expected for reaction rate–limited conditions. These results show that the experimental data can be accurately

GNP: gold nanoparticle

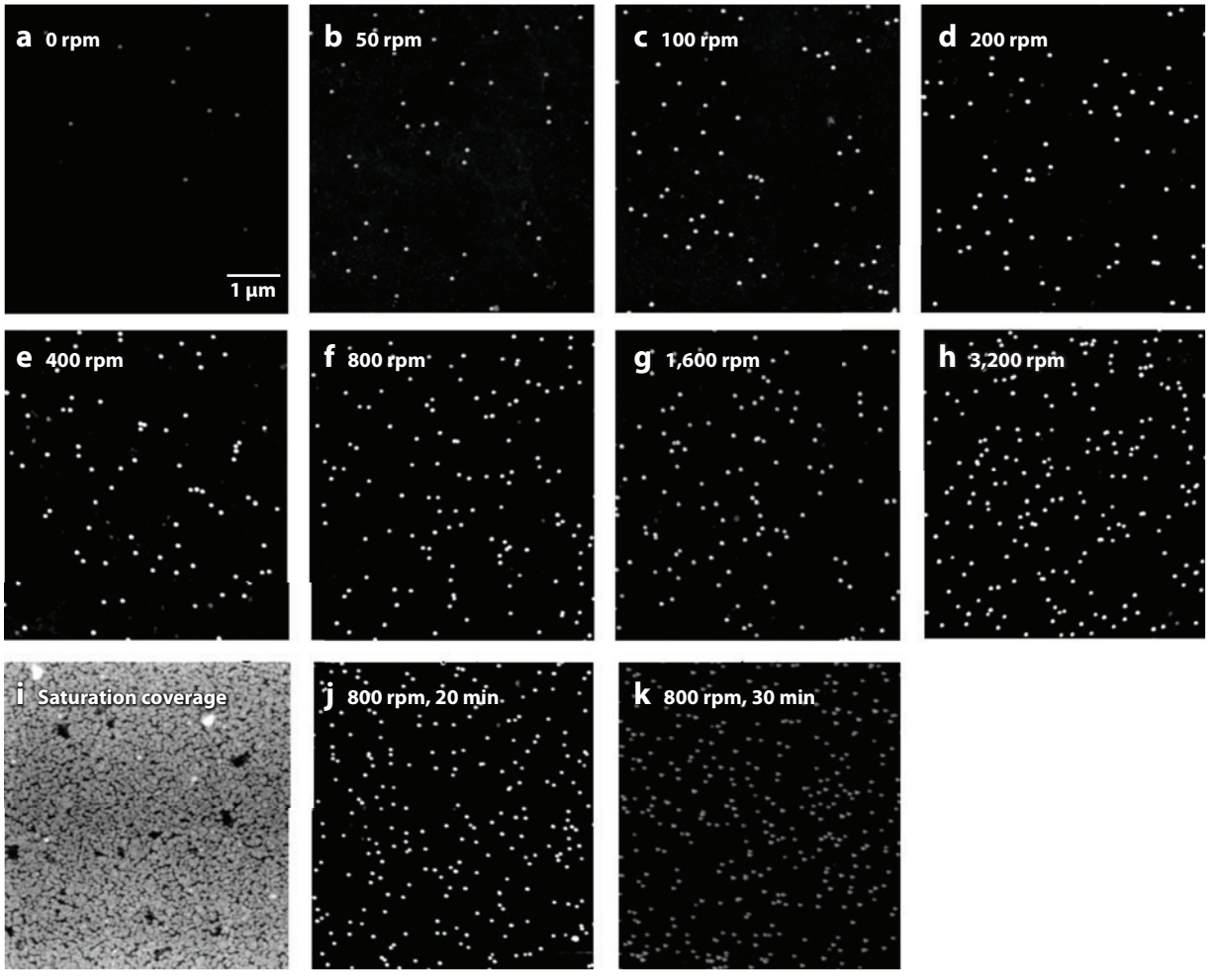

Figure 2

Atomic force microscopy images of 30-nm anti–mouse immunoglobin G (IgG) antibody–functionalized gold nanoparticles on mouse IgG–coated gold surfaces. (*a–b*) The substrate was rotated in nanoparticle suspensions of 3.6×10^9 particles ml^{-1} for 10 min. The rotation speeds were 0, 50, 100, 200, 400, 800, 1,600, and 3,200 rpm, respectively. (*i*) A capture surface was saturated with 30-nm gold nanoparticles by incubating in a high concentration of particles (3.6×10^{11} particles ml^{-1}) for an extended period (16 h). (*j*, *k*) The substrate was rotated at 800 rpm in 3.6×10^9 particles ml^{-1} suspension for 20 and 30 min, respectively. See Reference 74 for experimental details. Reproduced with permission from Reference 74. Copyright 2009, American Chemical Society.

modeled by Equation 22; this equation, rather than its abbreviated form (Equation 27), should therefore be used to deduce the metrics central to binding kinetics.

Equation 25 provides an approach with which to test the reliability of the theoretical model further by determining the values of D and k_{on} simultaneously. If the model is accurate, it should be possible to determine the values of D for the GNPs from the data in **Figure 2**. **Figure 4** graphs tC_b/Γ as a function of $1/\omega^{1/2}$ for the captured GNPs. The plot reasonably follows a linear relationship with a nonzero intercept, indicating the binding follows the reaction kinetics model. From the slope of the linear regression line, we calculate D for the 30-nm GNPs to be 1.8×10^{-11} m^2 s^{-1}. The product $k_{on}S^0_{Ab}$ (i.e., the inverse of the intercept) is 5.6×10^{-6} m s^{-1};

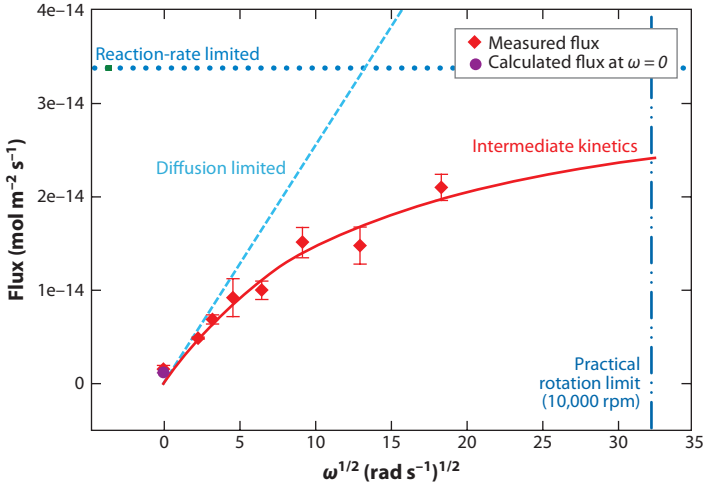

Figure 3

Flux of gold nanoparticles as a function of the square root of the rotation speed $\omega^{1/2}$. Trend lines (*dashed blue lines*) indicate the reaction rate–limited flux (see Equation 28) and diffusion rate–limited flux (see Equation 27), calculated via the parameters determined here. The solid red line is a plot of Equation 22 that uses the experimentally determined binding kinetics parameters, extrapolated to the practical upper limit of rotation speed. A previously determined value of $k_{on}S^0_{Ab}$ (5.6×10^{-6} m s^{-1}) was used. Note that the calculated and observed flux at $\omega^{1/2} = 0$ coincide with each other (74). Reproduced with permission from Reference 74. Copyright 2009, American Chemical Society.

we refer the reader to a recent publication (74) for an analysis of these data to deduce a value for k_{on}.

To check the value of D, the Stokes-Einstein equation was used to calculate the hydrodynamic diameter of the GNPs. The result is 24.7 nm, which closely matches the average diameter found

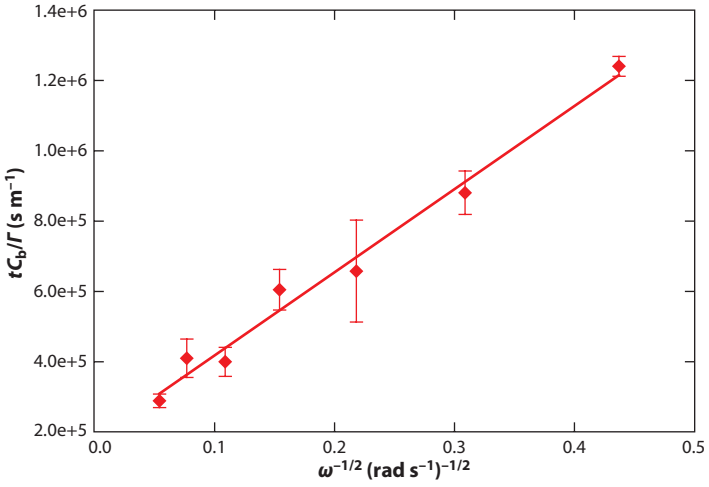

Figure 4

Plot of the product of time and the ratio of gold nanoparticle concentration to surface coverage (tC^b/Γ) as a function of the inverse of the square root of the rotation rate ($1/\omega^{1/2}$). The data points follow a straight line, indicating the correctness of the binding kinetics model (Equation 23). Reproduced with permission from Reference 74. Copyright 2009, American Chemical Society.

from AFM imaging, 25.4 ± 2.9 nm. Importantly, this level of agreement (see Reference 74 for details) validates the theoretical basis for antibody-antigen binding kinetics. These results begin to demonstrate that a rotating capture substrate can serve as a simple tool not only to accelerate assay time but also to probe key fundamental parameters in assay reaction kinetics.

PPV: porcine parvovirus

4. APPLICATIONS OF A ROTATING CAPTURE SUBSTRATE

4.1. Atomic Force Microscopy–Based Label-Free Immunoassay for Porcine Parvovirus

This subsection demonstrates the ability of capture substrate rotation to reduce incubation time while maintaining a high level of analytical performance (e.g., LOD) via realistic samples and matrices. To this end, capture substrates modified with monoclonal antibodies for porcine parvovirus (PPV) were exposed to sample solutions of PPV (3.2×10^6 $TCID_{50}$ ml^{-1}, where $TCID_{50}$ refers to 50% tissue-culture infective dosage) as a function of ω and t and were then imaged by AFM to enumerate PPV accumulation (72). PPV appeared as a spherical object with a height of ~18 nm. The height of the imaged PPV is consistent for all the particles (76) but is slightly smaller than expected, which is attributed to dehydration of the ~25-nm viral particles after drying.

Figure 5 plots Γ against ω for 10- and 30-min incubations. Rotation rates up to 1,200 rpm were tested. Rotation clearly yielded a significant increase in the number of captured viruses for both incubation times. Not surprisingly, the 30-min incubations led to increased accumulation of PPV on the immunosubstrate as compared to the 10-min incubations rotated at the same speeds. Importantly, the shape of each curve paralleled that expected for accumulation influenced by mass transport. The data can be accurately fit to Equation 23, which shows that the binding kinetics for a larger analyte can be quantitatively analyzed as well as manipulated to decrease assay time.

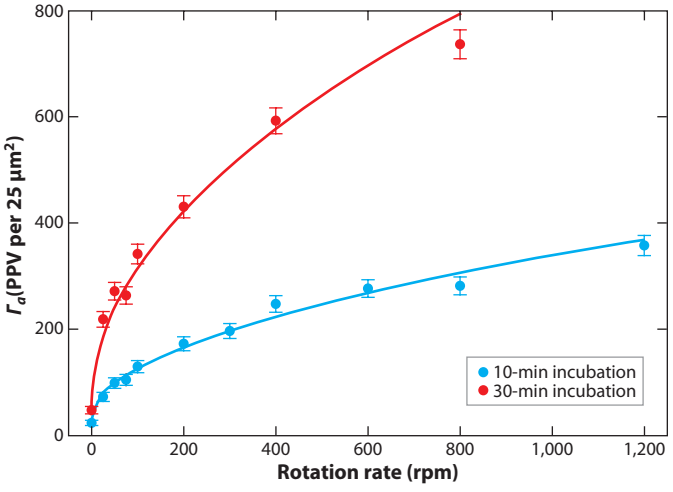

Figure 5

The number of porcine parvovirus (PPV) particles bound to the capture substrates at varying rotation rates is plotted. Each plot is constructed from the average of two to three substrates at each rotation rate. Five atomic force microscopy images from each capture substrate were collected. The error bars represent the errors introduced through Poisson statistics, and the solid lines represent weighted fits of the experimental data to Equation 23. Reproduced with permission from Reference 72.

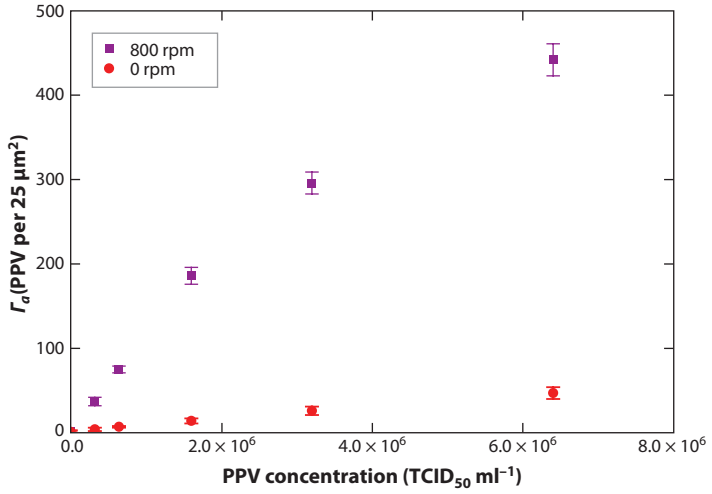

Figure 6

Dose-response curves for immunoassays performed under stagnant conditions and with capture substrate rotation at 800 rpm. The sample volume was 1.0 ml, and the incubation time was 10 min. Each data point is the average signal measured from five different locations on the same sample substrate, and the standard deviations are represented by the error bars. Abbreviation: PPV, porcine parvovirus. Reproduced with permission from Reference 72.

To demonstrate the analytical value of rotation-induced flux for an immunoassay, two sets of PPV binding experiments were carried out (72): one without substrate rotation and the other with rotation at 800 rpm. Dose-response curves were constructed by exposure of capture substrates to varying concentrations of PPV diluted in 10 mM PBS (phosphate-buffered saline) and through use of AFM for enumeration. All incubation times were held at 10 min. **Figure 6** plots the results. The immunoassay performed with substrate rotation is clearly much more sensitive than the immunoassay that relied solely on diffusion. A much longer incubation (~12 h) is required for stagnant incubations to reach equivalent values of Γ. Again, the assay at 800 rpm was carried out in 10 min. A few virus-sized objects were found in the images of blanks; these were attributed to debris with a size comparable to PPV. On the basis of these results, the LOD, which is defined as the concentration yielding a signal equal to the blank signal plus three times its standard deviation, was determined to be 3×10^5 TCID$_{50}$ ml^{-1} without rotation and 3×10^4 TCID$_{50}$ ml^{-1} with rotation at 800 rpm.

4.2. Standard-Free Quantification of Viral Particles

The adherence of PPV binding to the mathematical model for rotationally induced flux results in a unique and valuable application: Rotationally induced flow facilitates the accurate determination of virus concentration without the use of standards. Typically, infectious and hemagglutination titration and plaque assays are used to determine approximate virus titers in units of TCID$_{50}$, hemagglutination units, or plaque-forming units (77). Although these approaches are highly valuable, concentrations of virus particles represent a more effective means for assessment of assay performance and, ultimately, diagnostic utility (78).

Stagnant incubation: assay in which only diffusional mass transport is responsible for the delivery of antigen to the sensor surface

At present, transmission electron microscopy (TEM) is the standard method for measuring virus concentration (78). However, the reliable implementation of this approach requires highly purified virus solutions and the accurate transfer of small sample volumes to the TEM grid. The

analysis of the images also assumes that the virus is homogeneously distributed across the dried sample. The combined weight of these factors severely limits the reliability of this method (78).

A rotating capture substrate overcomes these obstacles. Imaging and enumerating the bound PPV with respect to ω and t can quantify the solution concentration of viral particles via Equation 27. This technique can then be used to determine the relationship between a measured titer (e.g., $TCID_{50}$) and viruses per unit volume with much less sample pretreatment, lower-cost instrumentation, fewer reagents, and a significant reduction in time.

To demonstrate this application, we analyzed the data in **Figure 5** with respect to Equation 25 by plotting t/Γ as a function of $1/\omega^{1/2}$. The slope of the linear regression yields the product $C_b D^{2/3}$, from which we determined the bulk solution virus concentration to be 7.6×10^9 viruses ml^{-1} by assuming a hydrodynamic diameter of PPV of 25 nm (79). For comparison, we previously determined the concentration to be $4.6–4.9 \times 10^9$ viruses ml^{-1} through experiments based on the exhaustive extraction of PPV from a sample solution (72).

Sandwich immunoassay: two-step assay in which (*a*) the antigen first binds to the antibody and (*b*) a labeled secondary antibody binds to the captured antigen for indirect detection

Extrinsic Raman label (ERL): a SERS tag for antigen detection consisting of a gold nanoparticle modified with a Raman reporter molecule and a labeling antibody

DSNB: 5,5′-dithiobis(succinimidyl-2-nitrobenzoate)

4.3. Surface-Enhanced Raman Scattering–Based Sandwich Immunoassay for Rabbit Immunoglobin G

The rotating capture substrate approach can be used to expedite both the antigen-binding and the antigen-labeling steps in a sandwich immunoassay. To this end, we performed an assay for rabbit IgG protein that used extrinsic Raman labels (ERLs) in the second step to read out the antigen concentration by SERS. In this assay, a capture substrate specific for rabbit IgG was prepared and incubated under either static or rotating conditions. Subsequently, the substrates were exposed to ERLs under static or rotating conditions. ERLs consist of a GNP to provide the surface enhancement, modified with both an antibody to specifically label the captured antigen and an inherently strong Raman reporter molecule such as 5,5′-dithiobis(succinimidyl-2-nitrobenzoate) (DSNB) to provide the Raman signal. Reference 74 details the effect of rotation on both the binding and labeling steps and the differences between the two. For example, the difference between the values of D for the protein and for the ERL, as well as the difference between binding-site vacancies, resulted in different contributions from kinetic binding and mass-transport limitations in each step. Ultimately, conditions were determined in which the incubation time for each step under rotation was minimized, and the analytical performance of the assay was maintained as compared to 12-h stagnant incubations.

An anti–rabbit IgG capture substrate was prepared and incubated with varying concentrations of antigen for 12 h under stagnant conditions, following a blocking step. The bound antigen was labeled with a rabbit IgG–specific ERL with a 12-h stagnant incubation. The SERS spectra for each of the sample concentrations are displayed in **Figure 7**. The spectral signature is consistent with the Raman spectrum of DSNB, the Raman reporter molecule used to construct the ERL. The figure shows that the spectral intensity increases as the concentration of rabbit IgG increases, due to the binding of more ERLs. Quantitative information regarding the analyte concentration is obtained by a dose-response curve in which the intensity of the band at 1,336 cm^{-1} due to the symmetric NO_2 stretch is plotted as a function of analyte concentration (**Figure 8**). This assay was used as a control compared with the assay with substrate rotation (800 rpm). Optimization showed that a 10-min sample incubation and a 15-min label incubation closely matched the SERS response for the stagnant assay with the two 12-h incubation steps. Both sets of data are shown in **Figure 8**.

Several noteworthy observations can be made from the two curves. Although the responses for the two assays are nearly equivalent, the assay with rotation was performed in 25 min, whereas that of the standard (i.e., quiet) assay ran for 24 h. Thus, the use of rotation yields a significant (nearly

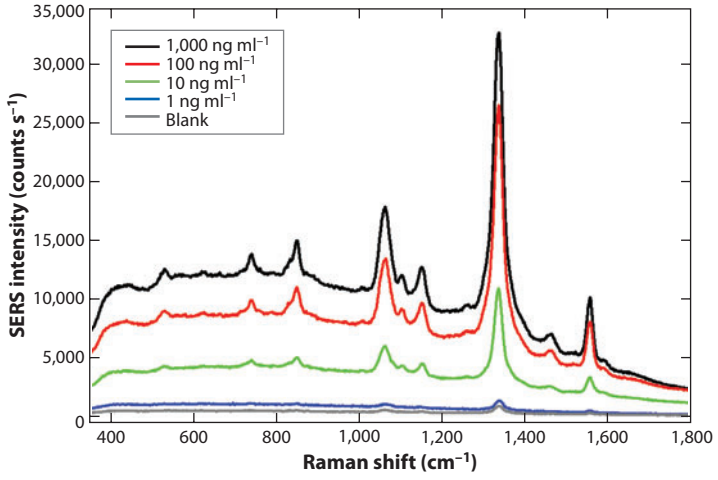

Figure 7

Surface-enhanced Raman scattering (SERS) spectra for the detection of rabbit immunoglobin G samples obtained from a 12-h sample and extrinsic Raman label stagnant incubations. Reproduced with permission from Reference 73. Copyright 2007, American Chemical Society.

60-fold) reduction in assay time without a loss of sensitivity. Furthermore, the level of nonspecific binding for the rotated substrate is less than the level obtained under stagnant conditions, which reduces the LOD. The LOD for the assay without rotation is ~10 ng ml^{-1}, whereas that for the assay with rotation is approximately 10-fold lower (~1 ng ml^{-1}). Ultimately, rotation reduced

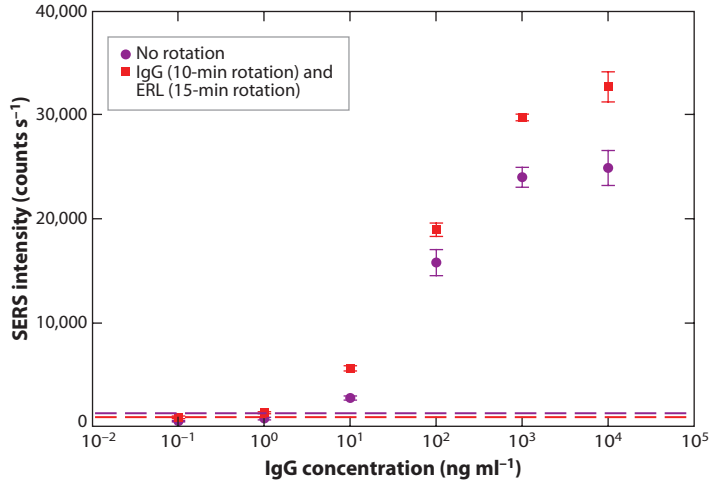

Figure 8

Dose-response curves for the surface-enhanced Raman scattering (SERS)-based detection of rabbit immunoglobin G (IgG), comparing the results for a control assay requiring 24 h (12-h capture step and 12-h labeling step) to those obtained with optimized rotation (800 rpm) performed in 25 min (10-min capture step and 15-min labeling step). The SERS intensity is that of the symmetric nitro stretch (υ_s; NO_2) at 1,336 cm^{-1}. The dashed lines represent the lowest detectable signal (blank signal plus three times its standard deviation) for each assay. Abbreviation: ERL, extrinsic Raman label. Reproduced with permission from Reference 73. Copyright 2007, American Chemical Society.

each incubation step in a two-step sandwich assay while improving the analytical performance, a feat that is not typically attainable.

4.4. Reducing Nonspecific Binding

Nonspecific binding results from off-target analytes and/or the label sticking to the capture substrate, yielding a false positive response, which ultimately limits the diagnostic reliability of immunoassays. Indeed, a host of steps, such as use of blocking agents, can be taken to minimize nonspecific binding. Such strategies can reduce, but often cannot eliminate, the background signal. This issue is becoming more important as readout technologies become more sensitive, accentuating the need to distinguish whether the signal equivalent to a single binding event is due to the analyte or nonspecific binding. Thus, methods to reduce or eliminate nonspecific binding will prove pivotal to the ability to exploit the sensitivity of many existing and emerging readout platforms.

Although specific interactions have been observed to proceed at a rate above that of mass transport, nonspecific binding is typically much slower and therefore is not diffusion limited. Nonspecific binding occurs because the label has restricted lateral diffusion in the vicinity of the capture surface (80), which allows for the accumulation of many weak interactions (e.g., electrostatic, Van der Waals, and Lewis acid-base forces) among the antigen, label, and capture substrate. The level of nonspecific binding therefore depends on the rate of accumulation of these interactions (47). Because nonspecific binding is not mass-transport limited, an increase in antigen and label flux will probably have a greater impact on the specific accumulation of the target species as opposed to off-target moieties.

To test this assertion, we incubated capture substrates specific for mouse IgG with human IgG, an off-target analyte. The substrates were then exposed to a suspension of anti–mouse IgG antibody–modified ERLs. Thus, any detectable SERS signal originated from the nonspecific binding of ERLs to either the capture antibodies or the bound antigen. **Figure 9** shows the results

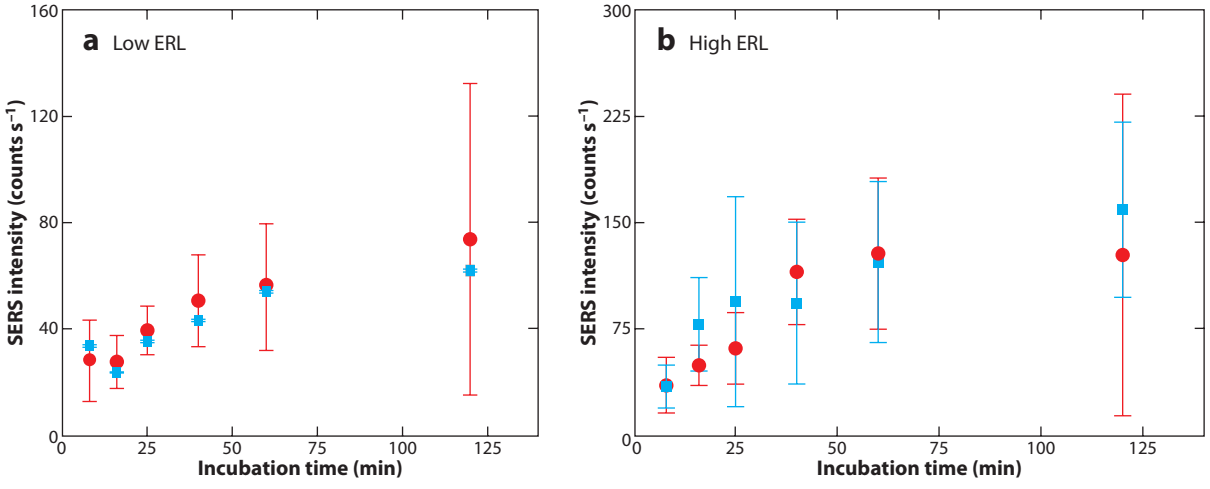

Figure 9

Plots of surface-enhanced Raman scattering (SERS) background intensity versus incubation time for both rotation (*red circles*) and stagnant (*blue squares*) incubations in extrinsic Raman labels (ERLs). (*a*) Low ERL is the response from substrates exposed to a solution containing 4.2×10^{10} particles ml^{-1}. (*b*) High ERL is the response from substrates exposed to a solution containing 9.4×10^{10} particles ml^{-1}. Prior to ERL exposure, substrates were incubated with 20-μl drops of 100 ng ml^{-1} human immunoglobin G for ~16 h.

of experiments that used two different label concentrations. The plots show that rotation has little effect on nonspecific ERL binding. Moreover, rotation increases the rate of specific binding (i.e., antigen and label binding) without increasing that of nonspecific binding. These data further substantiate the fact that capture substrate rotation not only decreases the time required for both incubation steps in SERS-based sandwich immunoassays but also decreases the level of nonspecific binding. The combined weight of both circumstances leads to shorter assays with improved LODs. We believe this result applies to virtually all types of assay formats.

5. SIMULATION OF BINDING KINETICS FOR IMMUNOASSAY DESIGN

The precise control of flux at a rotating capture substrate, coupled with an understanding of the theoretical underpinnings of the process, allows quantitative predictions of reactant accumulation with respect to time. As detailed elsewhere (74), models for such predictions are usually performed via numerical simulations. This section presents a few examples of how simulations can aid in understanding fundamental limitations in assay performance for a given set of conditions and in advancing assay design to meet specific performance metrics (e.g., LOD and analysis time).

Figure 10 presents the impact of differences in δ, achieved through rotation, on the accumulation of PPV on a 5 × 5 μm capture substrate as a function of t using previously determined kinetic parameters (74). A kinetic binding curve from diffusion (i.e., static solution) was also simulated via Equation 8. Clearly, the thinner the diffusion layer is, the faster the approach to equilibrium is. From simulations, we can compare the times needed to reach a given Γ. **Table 1** lists the theoretical times for a static assay as well as for assays at different rotation speeds to reach 1%, 5%, and 15% of the equilibrium surface concentration (Γ_E). It takes, for instance, 10 min at a rotation speed of 800 rpm and 28.5 h for static diffusion to reach 15% of Γ_E, an expediting factor of 166 for rotation assays! The table also shows that an additional increase in the rotation speed can further shorten incubation times, but to a much smaller extent.

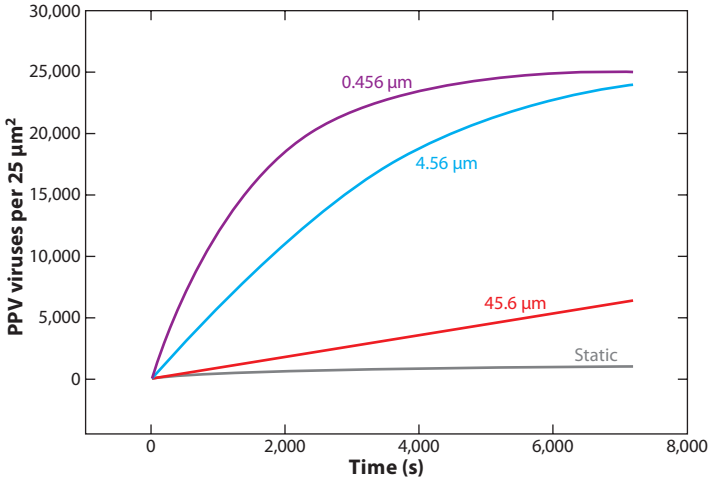

Figure 10

The effect of rotation speed on binding kinetics. Simulated porcine parvovirus (PPV) surface accumulation in a 5 × 5 μm area as a function of time and diffusion-layer thickness. The bulk virus concentration was assumed to be 1.0×10^{11} viruses ml^{-1}. Reproduced with permission from Reference 74. Copyright 2009, American Chemical Society.

Table 1 The effect of diffusion-layer thickness on binding time of porcine parvovirus

Rotation speed (rpm)	Diffusion-layer thickness (μm)	Damköhler number	Time to reach 1% equilibrium coverage (s)	Time to reach 5% equilibrium coverage (s)	Time to reach 15% equilibrium coverage (s)
Infinity	0	0	13	67	200
80,000	0.456	0.20	15	82	260
800	4.56	2.0	40	190	620
8	45.6	20	300	1,400	4,200
Static	–	–	460	11,000	10,000

Figure 11 shows the binding kinetics at different analyte concentrations. Simulated accumulations of PPV in a 5 × 5 μm area as a function of t and C^b are plotted in **Figure 11*a***. Significantly, at low concentrations (below 1.0×10^{11} viruses ml^{-1} or 166 pM), it takes an extremely long time to approach Γ_E, even at 800 rpm. In an additional illustration of the impact of concentration on binding rates, the times required for a rotation at 800 rpm to reach 50% of Γ_E at different PPV concentrations are plotted in **Figure 11*b***. The critical conclusion to draw from these results is that equilibrium is not reached on a practical time scale for low concentrations, and therefore the dose-response curve depends on t. **Figure 12*a*** shows time-dependent dose-response curves simulated for different incubation times at an 800-rpm rotation plotted on a semilog scale. The curve shifts to higher concentrations as t decreases, leading to a reduced sensitivity and an elevated LOD. This situation is clearly presented in **Figure 12*b***, which shows an expanded **Figure 12*a*** in the low-concentration range on a linear scale. From these simulations we obtain an LOD of 2.0×10^6 viruses ml^{-1} (3.4 fM) for a 10-h incubation, compared to 8.0×10^7 viruses ml^{-1} (130 fM) for a 10-min incubation. This is only one of many examples of how such simulations can provide guidance for tailoring experimental parameters to satisfy conflicting assay priorities such as speed versus LOD.

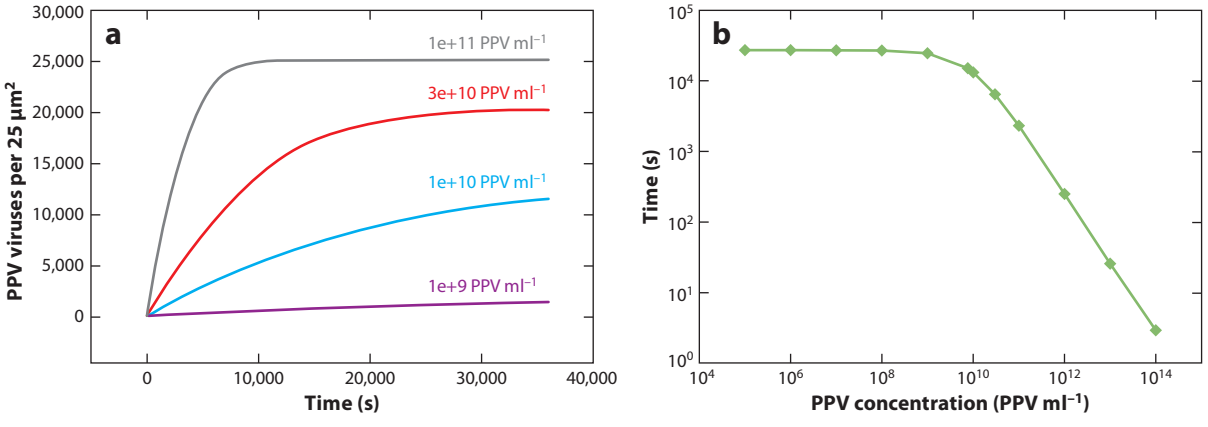

Figure 11

The effect of antigen concentration on binding kinetics. (*a*) Simulated porcine parvovirus (PPV) surface accumulation in a 5 × 5 μm area as a function of time at different PPV bulk concentrations. The rotation speed was assumed to be 800 rpm, resulting in a diffusion-layer thickness of 4.6 μm. (*b*) The time required to reach 50% equilibrium coverage at different concentrations. Reproduced with permission from Reference 74. Copyright 2009, American Chemical Society.

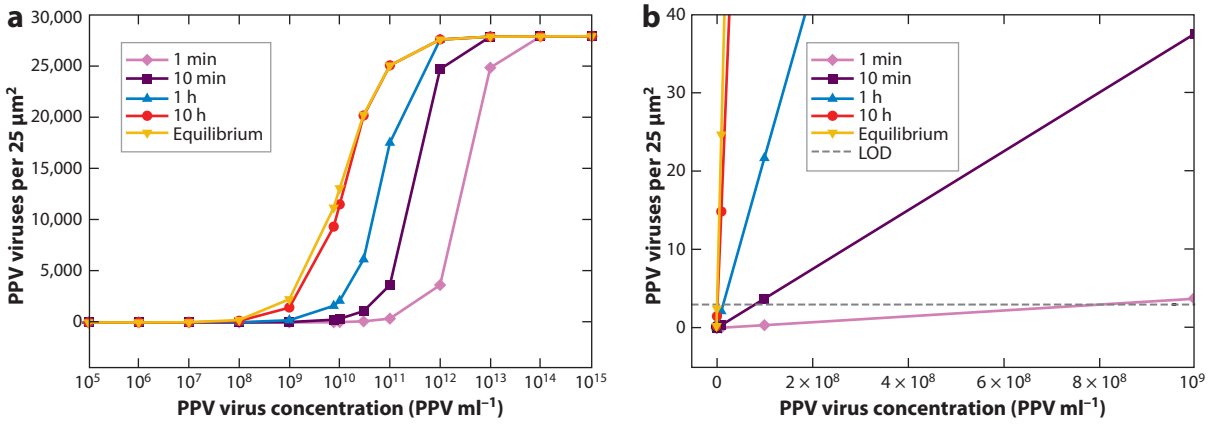

Figure 12

Incubation time dependency of porcine parvovirus (PPV) dose-response curves. (*a*) Simulated PPV surface accumulation in a 5 × 5 μm area as a function of PPV bulk concentration at different incubation times. (*b*) Expansion of panel *a* at low concentration on a linear scale. The rotation speed was assumed to be 800 rpm, corresponding to a diffusion-layer thickness of 4.6 μm. The dashed line is an assumed threshold of three viruses per image to differentiate analytes from background. Reproduced with permission from Reference 74. Copyright 2009, American Chemical Society.

6. CONCLUSIONS

This review details the first application of rotation-induced flux for the acceleration of antigen binding and labeling in heterogeneous immunoassays. The premise of the technique is that conventional heterogeneous immunoassay speed is usually limited by the rate of mass transport, that is, by diffusion of antigen to an antibody-coated surface. We have derived equations and solved the binding kinetics for antibody-antigen binding reactions on a rotating substrate surface. We found that by vigorously rotating the capture surface, the binding reaches the regime of intermediate binding kinetics, for which the rate of mass transport is comparable to the reaction rate. Systematic studies of the influence of rotation on antigen and label binding led to an optimized immunoassay that, in comparison to a stagnant assay carried out in 24 h, yielded in 25 min a 10-fold decrease in the LOD. Under these conditions, we can also determine the diffusion coefficient and reaction rate constant of the antigen.

Although specific antibody-antigen interactions are often considered to proceed at a rate above that of mass transport, nonspecific binding is typically much slower and not diffusion limited. Consistent with this observation, we found that rotation has little effect on nonspecific binding. Thus, rotation increases the rate of specific binding (i.e., antigen and label binding) without increasing that of nonspecific binding. The consequence is that capture substrate rotation not only decreases the time required for incubation but also decreases the level of nonspecific binding. The combined weight of both circumstances leads to shorter assays with improved LODs.

An interesting question is whether high rotation rates produce shear stresses (81, 82) that could damage proteins or viruses. The unfolding of proteins could expose hydrophobic regions and lead to aggregation. We have not observed any effects suggesting shear stress. AFM images of viruses captured during rotation showed no sign of damage, and assay results are consistent with the capturing of intact viruses. However, this is an issue that should be kept in mind when pushing the limits of rotation as a means for expediting immunoassays. Finally, although the merits of rotation-induced flow have been limited to AFM- and SERS-based immunoassays, this approach is amenable to all traditional and emerging readout modalities.

DISCLOSURE STATEMENT

R.J.L. and M.D.P. have interests in a company involved in SERS-based assays. The other authors are not aware of any affiliations, memberships, funding, or financial holdings that might affect the objectivity of this review.

ACKNOWLEDGMENTS

The authors gratefully acknowledge the vital contributions of past members of our research group. Portions of this work have been supported by the U.S. Department of Energy; the National Science Foundation; the National Institutes of Health; the U.S. Department of Agriculture; the National Aeronautics and Space Administration; the University of Utah; Iowa State University; and Concurrent Analytical, Inc.

LITERATURE CITED

1. Chomel BB. 2003. Control and prevention of emerging zoonoses. *J. Vet. Med. Educ.* 30:145–47
2. Diamandis EP, Christopoulos TK. 1996. Past, present, and future of immunoassays. In *Immunoassay*, ed. EP Diamandis, TK Christopoulos, pp. 1–3. San Diego: Academic
3. Liotta LA, Espina V, Mehta AI, Calvert V, Rosenblatt K, et al. 2003. Protein microarrays: meeting analytical challenges for clinical applications. *Cancer Cell* 3:317–25
4. Lueking A, Cahill DJ, Mullner S. 2005. Protein biochips: a new and versatile platform technology for molecular medicine. *Drug Discov. Today* 10:789–94
5. Cui Y, Ren B, Yao J-L, Gu R-A, Tian Z-Q. 2006. Synthesis of $Ag_{core}Au_{shell}$ bimetallic nanoparticles for immunoassay based on surface-enhanced Raman spectroscopy. *J. Phys. Chem. B* 110:4002–6
6. Petrik J. 2006. Diagnostic applications of microarrays. *Transfus. Med.* 16:233–47
7. Sokoll LJ, Chan KW. 1999. Clinical analyzers. Immunoassays. *Anal. Chem.* 71:356–62R
8. Patolsky F, Zheng GF, Hayden O, Lakadamyali M, Zhuang XW, et al. 2004. Electrical detection of single viruses. *Proc. Natl. Acad. Sci. USA* 101:14017–22
9. Patolsky F, Zheng GF, Lieber CM. 2006. Nanowire-based biosensors. *Anal. Chem.* 78:4260–69
10. Zheng GF, Patolsky F, Cui Y, Wang WU, Lieber CM. 2005. Multiplexed electrical detection of cancer markers with nanowire sensor arrays. *Nat. Biotechnol.* 23:1294–301
11. Smith EA, Corn RM. 2003. Surface plasmon resonance imaging as a tool to monitor biomolecular interactions in an array based format. *Appl. Spectrosc.* 57:320–32A
12. Mullett WM, Lai EPC, Yeung JM. 2000. Surface plasmon resonance–based immunoassays. *Methods* 22:77–91
13. Lyon LA, Music MD, Natan MJ. 1998. Colloidal Au–enhanced surface plasmon resonance immunosensing. *Anal. Chem.* 70:5177–83
14. Nelson BP, Grimsrud TE, Liles MR, Goodman RM, Corn RM. 2001. Surface plasmon resonance imaging measurements of DNA and RNA hybridization adsorption onto DNA microarrays. *Anal. Chem.* 73:1–7
15. Miyashita M, Shimada T, Miyagawa H, Akamatsu M. 2005. Surface plasmon resonance–based immunoassay for 17 B–estradiol and its application to the measurement of estrogen receptor–binding activity. *Anal. Bioanal. Chem.* 381:667–73
16. Gobi KV, Kataoka C, Miura N. 2005. Surface plasmon resonance detection of endocrine disruptors using immunoprobes based on self-assembled monolayers. *Sens. Actuator* 108:784–90
17. Sun B, Xie W, Yi G, Chen D, Zhou Y, et al. 2001. Microminiturized immunoassays using quantum dots as fluorescent label by laser confocal scanning fluorescence detection. *J. Immunol. Methods* 249:85–89
18. Goldman ER, Anderson GP, Tran PT, Mattoussi H, Charles PT, et al. 2002. Conjugation of luminescent quantum dots with antibodies using an engineered adaptor protein to provide new reagents for fluoroimmunoassays. *Anal. Chem.* 74:841–47
19. Goldman ER, Medintz IL, Mattoussi H. 2006. Luminescent quantum dots in immunoassays. *Anal. Bioanal. Chem.* 384:560–63

20. Hahn MA, Tabb JS, Krauss TD. 2005. Detection of single bacterial pathogens with semiconductor quantum dots. *Anal. Chem.* 77:4861–69
21. Faulds K, Smith WE, Graham D. 2004. Evaluation of surface-enhanced resonance Raman scattering for quantitative DNA analysis. *Anal. Chem.* 76:412–17
22. Chan WCW, Nie S. 1998. Quantum dot bioconjugates for ultrasensitive nonisotopic detection. *Science* 281:2016–18
23. Wu G, Datar RH, Thundat KMH, Cote RJ, Majumdar A. 2001. Bioassay of prostate-specific antigen (PSA) using microcantilevers. *Nat. Biotechnol.* 19:856–60
24. Grogan C, Raiteri R, O'Connor GM, Glynn TJ, Cunningham V, et al. 2002. Characterization of an antibody coated microcantilever as a potential immuno-based biosensor. *Biosens. Bioelectron.* 17:201–7
25. Llic B, Yang Y, Craighead HG. 2004. Virus detection using nanoelectromechanical devices. *Appl. Phys. Lett.* 85:2604–6
26. Butler JE. 2000. Enzyme-linked immunosorbent assay. *J. Immunoassay* 21:165–209
27. Driskell JD, Kwarta KM, Lipert RJ, Porter MD, Neill JD, et al. 2005. Low level detection of viral pathogens by a surface-enhanced Raman scattering based immunoassay. *Anal. Chem.* 77:6147–54
28. Grubisha DS, Lipert RJ, Park H-Y, Driskell J, Porter MD. 2003. Femtomolar detection of prostate-specific antigen: an immunoassay based on surface-enhanced Raman scattering and immunogold labels. *Anal. Chem.* 75:5936–43
29. Ni J, Lipert RJ, Dawson B, Porter MD. 1999. Immunoassay readout method using extrinsic Raman labels adsorbed on immunogold colloids. *Anal. Chem.* 71:4903–8
30. Dou X, Takama T, Yamaguchi T, Tamamoto H, Ozaki Y. 1997. Enzyme immunoassay utilizing surface-enhanced Raman scattering of the enzyme reaction product. *Anal. Chem.* 69:1492–95
31. Rohr TE, Cotton T, Fan N, Tarcha PJ. 1989. Immunoassay employing surface-enhanced Raman spectroscopy. *Anal. Biochem.* 182:388–98
32. Xu S, Ji X, Xu W, Li X, Wang L, et al. 2004. Immunoassay using probe-labeling immunogold nanoparticles with silver staining enhancement via surface-enhanced Raman scattering. *Analyst* 129:63–68
33. Mulvaney SP, Music MD, Keating CD, Natan MJ. 2003. Glass-coated, analyte-tagged nanoparticles: a new tagging system based on detection with surface-enhanced Raman scattering. *Langmuir* 19:4784–90
34. Zhang X, Young MA, Lyandres O, Duyne RPV. 2005. Rapid detection of an anthrax biomarker by surface-enhanced Raman spectroscopy. *J. Am. Chem. Soc.* 127:4484–89
35. Ansari DO, Stuart DA, Nie S. 2005. Surface enhanced Raman spectroscopic detection of cancer biomakers in intact cellular specimens. *Proc. SPIE* 5699:82–90
36. Cao YC, Jin R, Mirkin CA. 2002. Nanoparticles with Raman spectroscopic fingerprints for DNA and RNA detection. *Science* 297:1536–40
37. Faulds K, Barbagallo RP, Keer JT, Smith WE, Graham D. 2004. SERRS as a more sensitive technique for the detection of labeled oligonucleotides compared to fluorescence. *Analyst* 129:567–68
38. Graham D, Mallinder BJ, Whitcombe D, Smith WE. 2001. Surface enhanced resonance Raman scattering (SERRS)—a first example of its use in multiplex genotyping. *ChemPhysChem* 12:746–48
39. Graham D, Mallinder BJ, Whitcombe D, Watson ND, Smith WE. 2002. Simple multiplex genotyping by surface-enhanced resonance Raman scattering. *Anal. Chem.* 74:1069–74
40. Jones VW, Kenseth JR, Porter MD, Mosher CL, Henderson E. 1998. Microminiaturized immunoassays using atomic force microscopy and compositionally patterned antigen arrays. *Anal. Chem.* 70:1233–41
41. Kenseth JR, Kwarta KM, Driskell JD, Porter MD, Neill JD, et al. 2007. Strategies in the use of atomic force microscopy as a multiplexed readout tool of chip-scale protein motifs. In *Combinatorial Materials Science*, ed. S Mallapragada, B Narasimhan, MD Porter, pp. 81–107. New York: Wiley
42. Lee KB, Kim EY, Mirkin CA, Wolinsky SM. 2004. The use of nanoarrays for highly sensitive and selective detection of human immunodeficiency virus type 1 in plasma. *Nano Lett.* 4:1869–72
43. Nettikadan SR, Johnson JC, Mosher C, Henderson E. 2003. Virus particle detection by solid phase immunocapture and atomic force microscopy. *Biochem. Biophys. Res. Commun.* 311:540–45
44. Takano H, Kenseth JR, Wong SS, O'Brien JC, Porter MD. 1999. Chemical and biochemical analysis using scanning force microscopy. *Chem. Rev.* 99:2845–90
45. Sheehan PE, Whitman LJ. 2005. Detection limits for nanoscale biosensors. *Nano Lett.* 5:803–7

46. Frackelton AR, Weltman JK. 1980. Diffusion control of the binding of carcinoembryonic antigen (CEA) with insoluble anti-CEA antibody. *J. Immunol. Methods* 124:2048–54
47. Kusnezow W, Syagailo YV, Rueffer S, Baudenstiel N, Gauer C, et al. 2006. Optimal design of microarray immunoassays to compensate for kinetic limitations. Theory and experiment. *Mol. Cell. Proteomics* 5:1681–96
48. Myszka DG, Morton TA, Doyle ML, Chaiken IM. 1997. Kinetic analysis of a protein antigen-antibody interaction limited by mass transport on an optical biosensor. *Biophys. Chem.* 64:127–37
49. Nygren H, Werthen M, Stenberg M. 1987. Kinetics of antibody binding to solid-phase-immobilized antigen: effect of diffusion rate limitation and steric interaction. *J. Immunol. Methods* 101:63–71
50. Stenberg M, Nygren H. 1985. A diffusion limited reaction theory for a solid-phase immunoassay. *J. Theor. Biol.* 113:589–97
51. Stenberg M, Stiblert L, Nygren H. 1986. External diffusion in solid-phase immunoassays. *J. Theor. Biol.* 120:129–40
52. Vijayendran RA, Ligler FS, Leckband DE. 1999. A computational reaction-diffusion model for the analysis of transport-limited kinetics. *Anal. Chem.* 71:5405–12
53. Luxton R, Badesha J, Kiely J, Hawkins P. 2004. Use of external magnetic fields to reduce reaction times in an immunoassay using micrometer-sized paramagnetic particles as labels (magnetoimmunoassay). *Anal. Chem.* 76:1715–19
54. Glaser RW. 1993. Antigen-antibody binding mass transport by convection and diffusion to a surface: a two-dimensional computer model of binding and dissociation kinetics. *Anal. Biochem.* 213:152–61
55. Hofmann O, Voirin G, Niedermann P, Manz A. 2002. Three-dimensional microfluidic confinement for efficient sample delivery to biosensor surfaces. Application to immunoassays on planar optical waveguides. *Anal. Chem.* 74:5243–50
56. Johnstone RW, Andrew SM, Hogarth MP, Pietersz GA, McKenzie IFC. 1990. The effect of temperature on the binding kinetics and equilibrium constants of monoclonal antibodies to cell surface antigens. *Mol. Immunol.* 27:327–33
57. Ewalt KL, Haigis RW, Rooney R, Ackley D, Krihak M. 2001. Detection of biological toxins on an active electronic microchip. *Anal. Biochem.* 289:162–72
58. Yang JM, Bell J, Huang Y, Tirado M, Thomas D, et al. 2002. An integrated, stacked microlaboratory for biological agent detection with DNA and immunoassays. *Biosens. Bioelectron.* 17:605–18
59. Pribyl M, Snita D, Hasal P, Marek M. 2004. Modeling of electric-field driven transport processes in microdevices for immunoassay. *Chem. Eng. J.* 101:303–14
60. Heller MJ, Forster AH, Tu E. 2000. Active microelectronic chip devices which utilize controlled electrophoretic fields for multiplex DNA hybridizaion and other genomic applications. *Electrophoresis* 21:157–64
61. Qian S, Bau HH. 2003. A mathematical model of lateral flow bioreactions applied to sandwich assays. *Anal. Biochem.* 322:89–98
62. Oku Y, Kamiya K, Kamiya H, Shibahara Y, Ii T, et al. 2001. Development of oligonucleotide lateral-flow immunoassay for multi-parameter detection. *J. Immunol. Methods* 258:73–84
63. Chan CPY, Sum KW, Cheung KY, Glatz JFC, Sanderson JE, et al. 2003. Development of a quantitative lateral-flow assay for rapid detection of fatty acid–binding protein. *J. Immunol. Methods* 279:91–100
64. O'Keeffe M, Crabbe P, Salden M, Wichers J, Peteghem CV, et al. 2003. Preliminary evaluation of a lateral flow immunoassay device for screening urine samples for the presence of sulphamethazine. *J. Immunol. Methods* 278:117–26
65. Fernandez-Sanchez C, McNeil CJ, Rawson K, Nilsson O. 2004. Disposable noncompetitive immunosensor for free and total prostate-specific antigen based on capacitance measurement. *Anal. Chem.* 76:5649–56
66. Al-Yousif Y, Anderson J, Chard-Bergstrom C, Kapil S. 2002. Development, evaluation, and application of lateral-flow immunoassay (immunochromatography) for detection of rotavirus in bovine fecal samples. *Clin. Diagn. Lab. Immunol.* 9:723–24
67. Slinger R, Milk R, Gaboury I, Diaz-Mitoma F. 2004. Evaluation of the QuickLab RSV test, a new rapid lateral-flow immunoassay for detection of respiratory syncytial virus antigen. *J. Clin. Microbiol.* 42:3731–33
68. Wittmann C, Bilitewski U, Giersch T, Kettling U, Schmid RD. 1996. Development and evaluation of a dipstick immunoassay format for the determination of atrazine residues on-site. *Analyst* 121:863–69

69. Bard AJ, Faulkner LR. 2001. *Electrochemical Methods: Fundamentals and Applications*. New York: Wiley
70. Opekar F, Beran P. 1976. Rotating-disk electrodes. *J. Electroanal. Chem.* 69:1–105
71. Reiger PH. 1994. *Electrochemistry*. New York: Chapman & Hall
72. Driskell JD, Kwarta KM, Lipert RJ, Vorwald A, Neill JD, et al. 2006. Control of antigen mass transfer via capture substrate rotation: an absolute method for the determination of viral pathogen concentration and reduction of heterogeneous immunoassay incubation times. *J. Virol. Methods* 138:160–69
73. Driskell JD, Uhlenkamp JM, Lipert RJ, Porter MD. 2007. Surface-enhanced Raman scattering immunoassays using a rotated capture substrate. *Anal. Chem.* 79:4141–48
74. Wang GF, Driskell JD, Porter MD, Lipert RJ. 2009. Control of antigen mass transport via capture substrate rotation: binding kinetics and implications on immunoassay speed and detection limits. *Anal. Chem.* 81:6175–85
75. Levich VG. 1962. *Physicochemical Hydrodynamics*. Englewood Cliffs: Prentice-Hall
76. Montelius L, Tegenfeldt JO. 1993. Direct observation of the tip shape in scanning probe microscopy. *Appl. Phys. Lett.* 62:2628–30
77. Murphy FA, Gibbs EPJ, Horzinek MC, Studdert MJ. 1999. *Veterinary Virology*. San Diego: Academic
78. Wagner EK, Hewlett MJ. 1999. *Basic Virology*. Malden, MA: Blackwell
79. Zadori Z, Szelei J, Tijssen P. 2005. SAT: a late NS protein of porcine parvovirus. *J. Virol.* 79:13129–38
80. Wild D, Kusnezow W. 2005. Separation systems. In *The Immunoassay Handbook*, ed. D Wild, pp. 187–89. New York: Elsevier. 3rd ed.
81. Biddlecombe JG, Craig AV, Zhang H, Uddin S, Mulot S, et al. 2007. Determining antibody stability: creation of solid-liquid interfacial effects within a high shear environment. *Biotechnol. Prog.* 23:1218–22
82. Maa YF, Hsu CC. 1997. Protein denaturization by combined effect of shear and air-liquid interface. *Biotechnol. Bioeng.* 54:503–12

Annual Review of
Analytical Chemistry

Volume 3, 2010

Contents

Indexes

Errata

An online log of corrections to *Annual Review of Analytical Chemistry* articles may be found at http://arjournals.annualreviews.org/errata/anchem.